

Choosing electrodes for deep brain stimulation experiments—electrochemical considerations

Jan Gimsa^a, Beate Habel^a, Ute Schreiber^b, Ursula van Rienen^b,
Ulf Strauss^c, Ulrike Gimsa^{c,*}

^a Department of Biology, University of Rostock, Chair of Biophysics, Gertrudenstr. 11A, D-18057 Rostock, Germany

^b University of Rostock, Faculty of Computer Science and Electrical Engineering, Chair of Theoretical Electrotechnics, Albert-Einstein-Str. 2, D-18059 Rostock, Germany

^c Department of Neurology, Medical Faculty, University of Rostock, Gehlsheimer Str. 20, D-18147 Rostock, Germany

Received 4 June 2004; received in revised form 27 July 2004; accepted 6 September 2004

Abstract

Deep brain stimulation (DBS) is a therapy of movement disorders including Parkinson's disease (PD). Commercially available electrodes for animal models of Parkinson's disease vary in geometry and material. We characterized such electrodes and found a drift in their properties within minutes and up to about 60 h after immersion in cell culture medium, both with and without a stimulation signal. Electrode properties could largely be restored by proteolytic treatment for platinum/iridium electrodes but not for stainless steel ones. Short-term drift and irreversible aging could be followed by impedance measurements. Aging was accompanied by metal corrosion and erosion of the plastic insulation. For both materials, the degradation rates depended on the current density at the electrode surfaces. Fourier analysis of the DBS pulse (60 μ s, repetition rate 130 Hz) revealed harmonic frequencies spanning a band of more than three decades, with significant harmonics up to the MHz range. The band is located in a window imposed by electrode processes and capacitive cell membrane bridging at the low and high frequency ends, respectively. Even though electrode processes are reduced at higher frequencies they only vanish above 1 MHz and cannot be avoided. Therefore, the use of inert electrode materials is of special importance. The neurotoxicity of iron makes avoiding stainless steel electrodes imperative. Future developments need to avoid the use of corrosive materials and current density hot spots at the electrode surface, and to reduce low frequency components in the DBS pulses in order to diminish electrode processes.

© 2004 Elsevier B.V. All rights reserved.

Keywords: High-frequency stimulation; Neuromodulation; Concentric electrodes; Current–voltage characteristics; Corrosion; Parkinson's disease

1. Introduction

Unlike other therapies, DBS was not preceded by extensive work in animal models. Consequently, its underlying mechanisms are still a matter of debate. While commercial electrodes for use in humans are highly standardized, there is no such standardization of the electrodes used in rodents or non-human primates. In addition, no data has so far been published that describes the commercial electrodes for human use, their properties and the field they induce in the target tissue—the central nervous system (CNS). We have charac-

terized electrodes of different materials and geometries that could be used in the DBS of rats.

Electrochemists have been dealing actively with the properties of electrodes and electrode processes since the 19th century (M. Faraday, *Experimental Researches in Chemistry and Physics*, 1859). Accordingly, a vast knowledge on the related electrochemical processes exists (Atkins, 1991). Nevertheless, electrode processes are extremely complex. This is reflected in the serious pursuit of the idea of cold nuclear fusion in the electrode reaction (Fleischmann et al., 1989). The possible combinations of electrode materials and solutions containing different ions and organic compounds are immense. Most data are available on the electrochemical behavior of electrodes in inorganic solutions or in commonly

* Corresponding author. Tel.: +49 381 4949608; fax: +49 381 4944889.
E-mail address: ulrike.gimsa@med.uni-rostock.de (U. Gimsa).

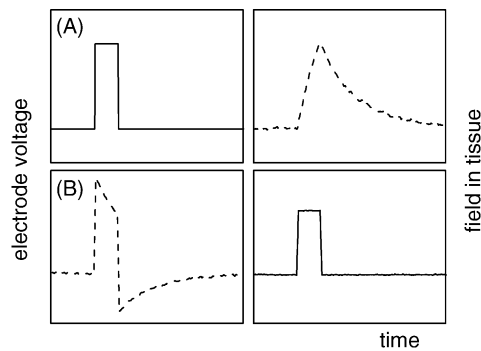


Fig. 1. Different modi for electric stimulation induce different field traces in the tissue. The solid line figures are applied electrode voltage and current pulses for constant-potential (A) and constant-current stimulation (B) by $60\ \mu\text{s}$ pulses, respectively. The dashed line figures are the resulting recorded signals. Electrode voltage and voltage drop over a shunt resistor were recorded by a two-channel Hewlett-Packard oscilloscope (HP54600A). The voltage drop over the shunt is proportional to the electrode current and thus to the time function of the field in the tissue (right figures). The scaling is arbitrary. The amplitude for the constant-voltage pulse was chosen to allow for direct comparability.

used buffers, such as phosphate buffered saline (PBS). Very few details are known of physiologically relevant media containing various ions and complex organic compounds.

In DBS, monophasic or biphasic needle pulses with a repetition frequency of 130 Hz and a pulse duration of $60\ \mu\text{s}$ are commonly used. While the DBS stimulators for use in humans operate in constant voltage mode, constant-current stimulation with square-topped signals with $500\ \mu\text{A}$ and a pulse width of approximately $60\ \mu\text{s}$ is commonly applied for DBS in laboratory animals (Windels et al., 2000; Meissner et al., 2000; Paul et al., 2000; Bruet et al., 2001; Meissner et al., 2001; Bressand et al., 2002; Chang et al., 2003; Moser et al., 2003; Windels et al., 2003). The actual time behavior of the electric field in the solution or tissue is proportional to the electrode current. For this reason, the constant-current mode generates a field which is independent of voltage drops at the electrodes, so preserving the wave shape of the current even for complex periodic signals. In constant-current mode the electrodes are driven by a voltage function correcting for the energy dissipation by electrode processes. Resulting differences are shown in Fig. 1. Fig. 1A shows the field in the tissue induced by constant-potential stimulation with a square-topped voltage signal while Fig. 1B shows the voltage signal used for constant-current stimulation to induce a square-topped field in the tissue. Interestingly, the constant-voltage pulse applied by the Kinetra[®] stimulator in PD patients resembles the voltage pulse shown in Fig. 1B (personal communication, M. Kienle, Medtronic Inc., Düsseldorf, Germany). The voltage function contains some “excess voltage” that is dissipated in electrode processes. These processes may result in electrochemical phenomena like gas evolution (hydrogen evolution at the cathode, oxygen and chlorine evolution at the anode), redox reactions of organic molecules, and the deposition of potentially harmful material, like metal

ions, chlorine and toxic organic products in the tissue. Metal dissolution will contribute to electrode corrosion and a subsequent change of electrode behavior over time. In contrast, the damage incurred on inserting the electrode into the brain tissue is negligible compared to the electrochemical electrode effects that may accompany DBS (Fung et al., 1998). Likewise, the shape of the electrode tip is of minor importance in relation to putative mechanical tissue damage although it is highly relevant with respect to the electric field distribution. Biphasic stimulation is aimed at balancing the effects of anodic and cathodic electrode reactions, such as pH alterations in the vicinity of the electrode. In rats, much less significant tissue damage has indeed been found when using biphasic rather than monophasic stimulation in DBS (Fung et al., 1998).

While toxic reactions limit DBS in the rat model with some electrodes but not with others (Darbaký et al., 2003), no or little tissue damage with chronic DBS has been observed in PD patients (Haberler et al., 2000; Henderson et al., 2002). Permanent iron deposits (one possible reason for tissue damage) have been detected in rats following stimulation with $1\ \mu\text{A}$ and using stainless steel electrodes for durations of as little as 5 s (Fung et al., 1998). This corresponds to 1.3 s of monophasic DBS. These observations indicate that electrode characterization is a prerequisite for successful work in animal models, in other words a valid modeling of the therapeutic effects in human patients.

This study combines classical electrochemical knowledge and experimental findings on the behavior of microelectrodes revealing problems which the scientific community should be aware of. It provides information on the optimization of the stimulating signal and on problems related to geometry and material. While this manuscript focuses on electrochemical electrode processes, the optimization of electrode geometry will be discussed elsewhere.

2. Materials and methods

2.1. Electrodes

Measurements were done on microelectrodes as commonly used for stimulation in rats. We investigated bipolar, coaxial microelectrodes of different stacked geometries and materials from different manufacturers (for details see Table 1). The poles of the electrode were isolated by epoxy. If possible in the experiments the outer pole was connected to ground potential. In the development of a first measuring setup and for comparison with the behavior of the microelectrodes platinum wire-electrodes with a diameter of 0.5 mm and an active length of 10 mm were used.

2.2. Electrolyte solutions

The electrolytes were artificial cerebro-spinal fluid (ACSF) containing 124 mM, 5 mM KCl, 1.25 mM NaH_2PO_4 ,

Table 1
Description of concentric bipolar electrodes used in our experiments

Electrode type	Abbreviation	Company	Material		Diameter (μm)		Pros	Cons
			Outer pole	Inner pole	Outer pole	Inner pole		
SNEX-100	Sx(b)	RMI	SS	SS	250	100	Widely used	Material; size ^a
CB CSG 75	S75-Pt/Ir	FHC	SS	Pt/Ir	250	75	Material	Price
CB CSH 75	S75-SS	FHC	SS	SS	250	75		Material
CB ASC 25	S25	FHC	SS	Pt/Ir	125	25	Material	Price; fragility

RMI: Rhodes Medical Instruments Inc., Tujunga, CA, USA. FHC: FHC Inc., Bowdoinham, ME, USA. SS: stainless steel. Pt/Ir: platinum/iridium.

^a Size should be appropriate for the target of stimulation. For the rat STN with an approximate size of 1 mm, an electrode diameter of 100 μm poses the risk of mechanical damage.

2 mM MgSO_4 , 26 mM NaHCO_3 , 2 mM CaCl_2 , 10 mM glucose; and cell culture medium (DMEM supplemented with 10% fetal calf serum (FCS; Biochrom, Berlin, Germany), 100 U/ml penicillin/streptomycin (Sigma, Deisenhofen, Germany), and 2.5 mM L-glutamine (Gibco BRL, Paisley, UK)). The conductivities of ACSF and cell culture medium were 1.42 and 1.40 S/m at 25 °C, respectively. All measurements were performed at room temperature of about 25 °C.

2.3. Electrode current–voltage behavior

A first electronic setup originally developed for experiments with wire-electrodes larger than those used in DBS has been adapted to the experiments with the DBS electrodes. We applied sinusoidal and pulsed signals in a constant-voltage mode to characterize the current–voltage relation and the electrode impedance. To generate the input voltage for DC and AC up to 1 MHz and to record the current voltage behavior, a DC power supply (50 V, Statron, Fürstenwalde, Germany) and a standard AC-generator (HP8116A, Hewlett-Packard, USA) have been used, respectively. The voltage drop over a shunt resistor and input voltage were recorded by a two-channel Hewlett-Packard oscilloscope (HP54600A) of 10 M Ω internal resistance. Since the temporal field shape in the medium is proportional to the current signal it could be obtained from the shunt resistor voltage. The electrode behavior could roughly be deduced from the difference in the shapes of driving voltage and current.

2.4. Electrode impedance characterization

In DBS in animal models mono- and biphasic signals, both consisting of rectangular needle pulses are usually applied. Typically, square wave pulses with a duration of 60 μs and a repetition rate of 130 Hz are used. (Please note that counting each pulse of a biphasic signal yields a pulse repetition rate of 130 Hz while the frequency is actually 65 Hz.)

For analysis of the electrode properties at 130 Hz we used a computer controlled HP 4194A impedance analyzer (Hewlett-Packard, MN, USA) to record the current voltage relation of the electrodes for two different modi. In a first series the impedance at 130 Hz has been recorded as a function of the DC bias. In this mode the DC bias was limited to

± 5 V by the impedance analyzer. For impedance detection at 130 Hz a sinusoidal AC signal of 10 mV_{pp} (mV peak to peak) amplitude was applied.

For the extremely steep slope (with respect to the signal period) of the needle pulses the Fourier series contains harmonic frequencies much higher than the basic frequencies of 65 or 130 Hz. Accordingly, the electrode behavior can only be properly described if electrode properties are known in a broad frequency band. In a second series of measurements we recorded the electrode impedance as a function of frequency in the range of 10^2 to 4×10^7 Hz. Again the AC signal had 10 mV_{pp}. DC bias voltages of 0, 100, and 500 mV were applied to alter the DC current density of the electrode.

3. Results and comments

3.1. Description of applied signal shape

To reveal which frequencies are actually contained in a pulsed field used for DBS, we modeled the pulse by a Fourier-series (Fig. 2). This analysis allowed us to separate the effects of high and low frequency components.

Fourier transformation allows for the decomposition of any periodic signal into a sum of harmonic sinusoidal and cosinusoidal functions. A general rule in rebuilding a proper pulse shape from a Fourier series is, the shorter the pulse width the higher the order of the harmonics of the fundamental frequency required (Eqs. (1) and (2)). This also applies to steep flanks.

Monophasic pulses $f(x) =$

$$\frac{2a}{\pi} \left[\frac{c}{2} + \frac{\sin c}{1} \cos x + \frac{\sin 2c}{2} \cos 2x + \frac{\sin 3c}{3} \cos 3x + \dots \right] \quad (1)$$

Biphasic pulses $f(x) =$

$$\frac{4a}{\pi} \left[\frac{\cos b}{1} \sin x + \frac{\cos 3b}{3} \sin 3x + \frac{\cos 5b}{5} \sin 5x + \dots \right] \quad (2)$$

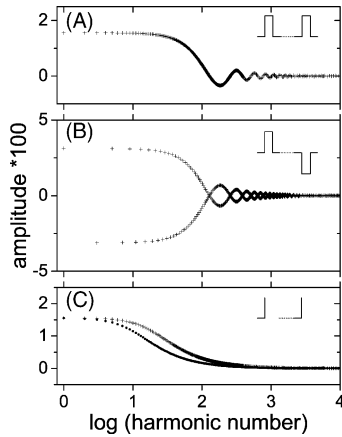


Fig. 2. DBS signals contain harmonics up to the MHz range. Fourier coefficients of typical signals used in DBS according to Eqs. (1–3). (A) Monophasic square wave pulse trace (duty cycle, 0.78%); (B) Biphasic square wave pulse trace (duty cycle, 0.78%); (C) Exponential decay pulse trace, normalized to the current integral, i.e. net charge, of the square wave pulses. Coefficients of two different signals are plotted (crosses: time constant equals pulse width, dots: pulse decaying to 1/1000 of its initial value within one period). Please note, that not all points were plotted at higher harmonic numbers due to the increasing point density over the logarithmic scale. Please note also, that in the DBS signals the basic frequency (harmonic number one) corresponds to 130 Hz for the monophasic (A) and 65 Hz for the biphasic (B) signal.

Exponential decay $f(x)$

$$= \frac{(1 - e^{-2\pi b})}{\pi b} \left[1 + \frac{1}{1 + (1/b)^2} \left(\cos x + \frac{1}{b} \sin x \right) + \frac{1}{1 + (2/b)^2} \left(\cos 2x + \frac{2}{b} \sin 2x \right) + \frac{1}{1 + (3/b)^2} \left(\cos 3x + \frac{3}{b} \sin 3x \right) + \dots \right] \quad (3)$$

with x being ωt (angular frequency, i.e. basic frequency of the Fourier series multiplied by time); and a , b , and c coding for the amplitude. For signals of 130 Hz with $60 \mu\text{s}$ pulse duration about 10^4 harmonics, i.e. frequencies up to 1.3 MHz, have to be considered to remodel a proper square wave pulse (compare to Fig. 3).

3.2. Electrode current–voltage behavior: the rookie approach

In our first experiments, conducted on millimeter-scale wire electrodes (further on referred to as macroelectrodes), we were able to roughly deduce the electrode properties from the difference in the shapes of the driving electrode voltage and the current. Standard textbook behavior (Vetter, 1961) could be reproduced (compare with solid bold line, Fig. 4). In electrolyte solution as well as in cell culture media, the current curve was characterized by a low slope for voltages that were below a characteristic value, bending up above this

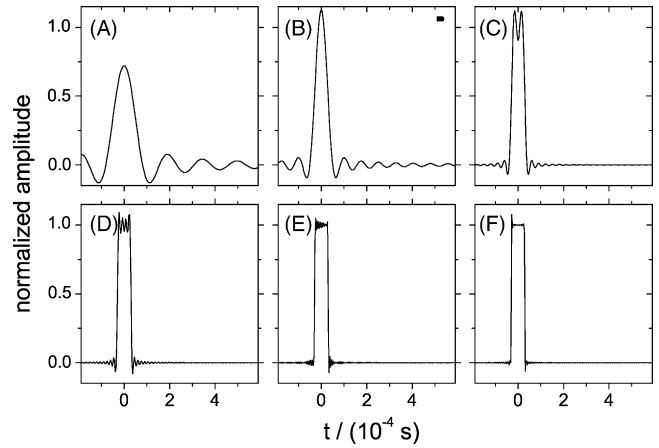


Fig. 3. A rectangular DBS pulse is comprised of its basic frequency (130 Hz) and higher harmonic frequencies. Fourier synthesis of a monophasic square wave pulse (duty cycle, 0.78%; compare to Eq. (1)). (A–F) present the resulting wave shape for the summation of: (A) 100; (B) 200; (C) 500; (D) 1000; (E) 2000; (F) 6000, harmonic frequencies. For the DBS pulse (F), corresponds to a summation up to 780 kHz.

value. Naturally, the two current branches were largely symmetrical with DC, i.e. independent of the polarity of the electrodes. With increasing frequency, this bending became less pronounced, and the slopes of both parts of the current function increased. Above a certain frequency the current function was linear, with the slope reflecting the DC conductance of the medium.

With DC, the characteristic “bending” voltage is known as the decomposition potential at which processes which are limiting the current flow are overcome by a further increase in voltage. Because of this non-linear behavior, a low frequency sinusoidal voltage with an amplitude higher than the decomposition potential generates a non-sinusoidal current (Schwan and Onaral, 1985). The current and the medium field signal contain higher harmonics of the basic frequency. At higher frequencies the non-linearity vanished because the electrode processes were capacitively bridged. Nevertheless, for a sinusoidal low frequency voltage signal or the low frequency components of a pulse signal, part of the electric energy will be dissipated by electrode reactions.

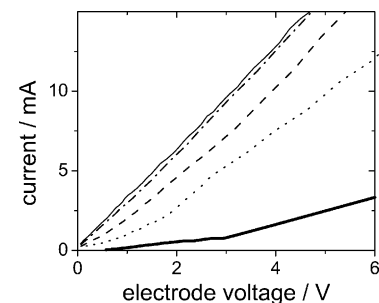


Fig. 4. Electrode processes are bridged at higher frequencies. Example for the current–voltage relation measured on platinum wire macroelectrodes in PBS with 10% FCS (bold solid line: DC; dotted line: 1 Hz; dashed line: 10 Hz; dash-dotted line: 100 Hz; thin solid line: 1 kHz). The 1 kHz curve solely corresponds to the medium resistance.

In order to allow the same setup to be employed in experiments with microelectrodes of higher impedance, the shunt resistor was adjusted to 1 M Ω . Surprisingly, this setup did not work properly. For DC, the characteristic bending in the slope around 2–3 V (see Fig. 4) could hardly be determined. The AC measurements suggested a very high shaft capacitance of about 200 pF (direct impedance measurements yielded about 20 pF). We assume that the reasons for these unexpected properties were threefold: high stray capacitances in the setup, a high current density due to the small active electrode areas, and unusual electrode behavior caused by a distribution of the current density along the active electrode surface. This non-uniform distribution results in a distribution of the intensity of the electrode reactions that leads to this unusual behavior. In the experiments, gas bubbles could be observed that were (in relation to the electrode size) much larger than in the case of the macroelectrodes. The intensity in the evolution of bubbles was correlated with the curvature of the electrodes. Because of the above difficulties, we looked for alternative ways to characterize the electrode behavior. In the literature, the properties as well as property changes of electrode–electrolyte interfaces are studied by cyclic voltametry or (as in our case) by frequency-domain electrochemical techniques (Schwan and Onaral, 1985; Macdonald, 1987).

3.3. Impedance spectroscopy

The major advantage of impedance spectroscopy is that effects can be examined at different experimental time scales within one experiment, depending on the frequency range that is swept. Nevertheless, given a non-linear electrode behavior, a sinusoidal voltage generates a current that may exhibit distortions from the sinusoidal shape. This effect makes impedance calculation by Ohm's law a complex problem since voltage and current functions will differ in shape. To obtain a largely linear current response we applied AC signals of very low amplitudes.

To analyze the impedance behavior of the electrodes we used four different media; deionized water, NaCl solution, ACSF and cell culture medium, of which the first three can be considered inorganic media, whereas the cell culture medium is rich in charged and non-charged organic molecules. ACSF on the other hand is a standard medium for in vitro electrophysiological recordings from neurons in brain slices, cell culture medium is closer to the in vivo conditions as it contains proteins as well as salts and sugars. To consider the difference between inorganic and organic media and the possible influence of macromolecule adsorption to the metallic electrode surface, we compared measurements in ACSF and cell culture medium throughout the paper.

Figs. 5 and 6 present alternative ways of plotting the complex chamber impedance. In Fig. 5 the imaginary part is plotted against the real part. The plots scale with medium conductivity. Accordingly, the plots at high medium conductivity are very similar to cell culture medium and ACSF. All plots consist of two typical sub-ranges: a straight line and a semi-

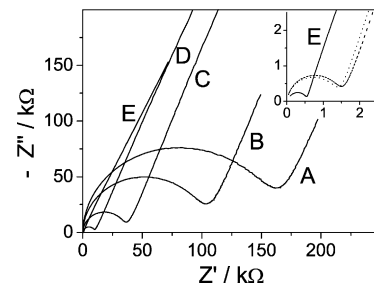


Fig. 5. Imaginary vs. real part of impedance. Conductivity dependence of typical impedance spectra for an S75-Pt/Ir electrode (Please note the negative sign of the ordinate): (A) 11.6 mS/m; (B) 18.6 mS/m; (C) 51 mS/m; (D) 185.6 mS/m; (E) 3.29 S/m NaCl solution. For each curve the frequency increases towards the origin. The transition frequency from the straight line into the semicircle indicates the cessation of electrode polarization processes (5 kHz, 9 kHz, 28 kHz, 113 kHz, and 1.99 MHz for A–E, respectively). It depends on medium (and electrode) properties. Inset: comparison of solutions of high ionic content. Solid line: 3.29 S/m NaCl solution (curve E), dashed line: cell culture medium, dotted line: ACSF. The resistance obtained by extrapolation of the low frequency end of the semicircles to the abscissa indicates the medium conductivity for a cell constant of 1.97 mm⁻¹.

circle. Zooming into the high conductivity spectra (Fig. 5, inset) qualitatively reveals the same curve shapes. The low frequency sub-range, straight line, belongs to the electrode, the semicircle to the medium impedances (see Section 4).

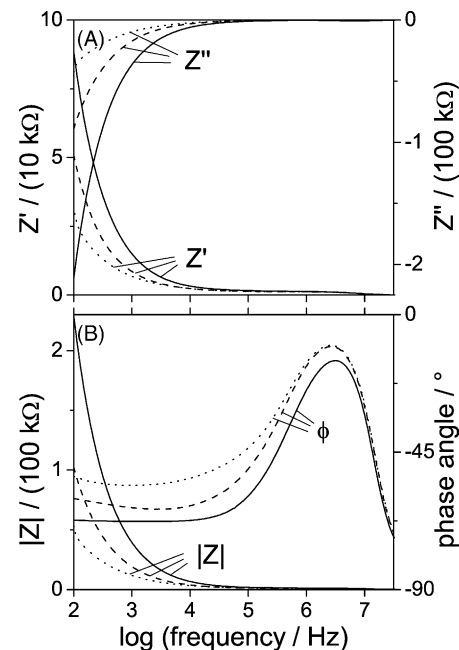


Fig. 6. Impedance vs. frequency for an S75-Pt/Ir electrode in cell culture medium measured at different DC biases (solid line: no bias; dashed line: 100 mV; dotted line: 500 mV). Relations must be compared to the inset in Fig. 5: (A) real (Z') and imaginary (Z'') parts; (B) absolute value ($|Z|$) and phase angle (Φ) of impedance. In this plot the phase angle is a sensitive parameter for the electrode properties (see electrode aging, Fig. 8). Please note that the peak in the phase angle around 2 MHz corresponds to the transition frequencies of Fig. 5. The impedance decreases for increasing bias. The plot suggests that frequency components below 1 kHz are largely blocked from contributing to the field in the solution by electrode processes. Only components above 1 MHz will be fully present in the medium.

Table 2
Dependence of characteristic parameters of the S75-Pt/Ir electrode immersed in NaCl solution on medium conductivity

Medium conductivity (mS/m)	Resistance at semicircle abscissa intercept (k Ω)	Frequency of line/semicircle transition (kHz)	Frequency at which medium impedance equals electrode impedance (kHz)
11.6	163	5	0.034
51	37.5	28	1.84
185.6	11	113	7.05
3290	0.6	1990	144

The semicircle-abscissa intercept (real part of impedance, see Fig. 5) represents the electrode resistance generated by the ionic medium conductivity. This resistance was used to calculate the frequency at which the driving voltage evenly contributes to electrode processes and field in the medium. Electrode processes cease at the frequency of line/semicircle transition.

Table 2 shows the frequencies at which the straight line transits into the semicircle, indicating the cessation of electrode processes. Circles were fitted to the semicircles to obtain the intercepts with the abscissa (column 2). The intercepts represent the resistances of the microelectrode/medium system generated by the ionic medium conductivity. As expected, the inverse intercept values linearly depend on conductivity, representing a cell constant (geometry factor) of about 1.97 mm^{-1} for the S75-Pt/Ir electrode.

In the linear sub-range of the plot, with increasing frequency the electrode processes are reduced. At a “break-even frequency” the driving voltage of the electrodes evenly contributes to electrode processes and field in the medium. A 1:1 voltage divider is formed by the electrode processes and the medium resistance, i.e. the absolute value of the impedance of the electrode processes is equal to the medium resistance. The break-even frequencies were estimated starting from the intercepts of the semicircles and the abscissa by determining the point at each curve that has the same distance from the intercept as the intercept to the origin. The frequencies obtained are given in column 4.

Fig. 6A presents the imaginary and real parts of the impedance over frequency for different DC biases. Fig. 6B presents the same data as the absolute value of the impedance (impedance modulus) and the phase angle over frequency. Capacitive properties are indicated by a negative phase angle. The angle approaches -90° for frequencies above that where the electrolyte resistance is superseded by the displacement current in the aqueous medium (see Section 4). In parallel, the impedance approaches zero. At low medium conductivities this behavior is more obvious in the complex plane (Fig. 5). Nevertheless, again at high medium conductivities, the phase angle provides a sensitive parameter for the electrode properties, e.g. reflecting the aging of the electrode surfaces (see Fig. 8). An increasing DC bias resulted in decreasing impedance, caused by the current density increase through the electrode surface. With increasing current densities, the modulus as well as the phase angle of impedance decreased.

3.4. Impedance at 130 Hz depends on bias voltage

The dependence of the impedance at 130 Hz on bias voltage has been recorded in cell culture medium and ACSF

(Fig. 7). To ensure detection of the impedance in the linear current–voltage range, a very small 130 Hz AC-signal voltage was applied using the impedance analyzer. The detected impedance strongly depended on the bias voltage and decreased for a higher bias. Obviously, the transit of charge carriers through the electrode surface becomes a more efficient process at higher current densities. This finding can be interpreted by an activation energy behavior where the bias supplies additional energy allowing the 130 Hz signal to induce a larger current through the electrode.

Fig. 7A presents the impedance at 130 Hz as a function of the bias voltage. Ohm’s law was used to calculate the fictive current–bias relation plotted in Fig. 7B. Interestingly, the

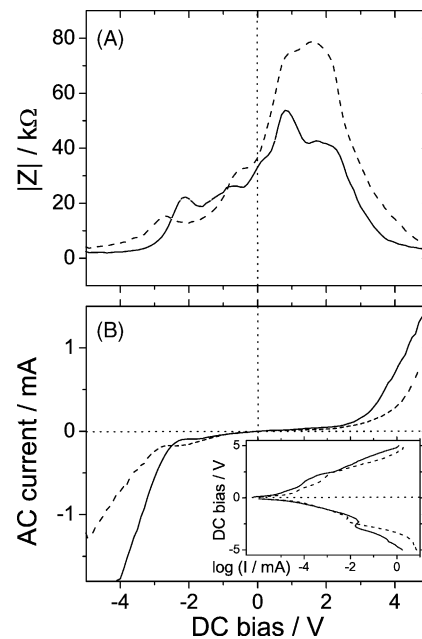


Fig. 7. Impedance dependence on DC bias for an S25-Pt/Ir electrode for two measuring solutions (solid line: ACSF; dashed line: cell culture medium): (A) electrode impedance for a sinusoidal signal (130 Hz, 10 mV); (B) the current–bias relation recalculated from (A) results in a curve qualitatively similar to those in Fig. 4. Obviously, the DC-bias introduces an additional energy, decreasing the impedance at 130 Hz. Please note, that the curve is asymmetric for positive and negative biases. Despite of the non-monotonous impedance behavior the shape of the recalculated current curve qualitatively corresponds to a typical current–voltage relation. Inset: recalculated Tafel-plot (bias voltage vs. logarithm of current) of B. In the Tafel-plot linear sections present reaction rates for certain compounds, like hydrogen, oxygen and chlorine evolution.

curve is asymmetric for positive and negative biases. Despite the irregular, non-monotonous impedance behavior, the shape of the recalculated current curve qualitatively corresponds to a typical current–voltage relation as seen for macroelectrodes (Fig. 4). The slopes of the current curves are different with the positive and the negative voltage branches. This means that different currents were measured for a given voltage when the inner or outer poles of the electrode had been used as the cathode. This behavior must be related to a current density dependence of the overpotentials (see below). In addition, the drastic increase above a specific electrode voltage (the bending point of the curves between 2 and 3 V) is asymmetric. The bending points depend on medium composition, electrode geometry, material, and surface properties (data not shown). The non-linear current–voltage relation implies that any slow AC signal driving the electrode and exceeding this characteristic potential will generate a field strength in the medium with a time dependence deviating from the input signal.

In addition a Tafel-plot, i.e. bias voltage versus logarithm of current (inset in Fig. 7B), was recalculated from the current-bias relation (Fig. 7B). In the Tafel-plot, linear sections present reaction rates for certain compounds, such as hydrogen, oxygen and chlorine gas evolution.

3.5. Long-term alterations and corrosion of electrodes

To study the long-term effects of electrochemical reactions and macro-molecular adsorption, the electrodes underwent about 30 min of impedance measurements before they were put into electrolyte solution for 5 days. Examples of impedance spectra are shown in Fig. 8. The spectra were recorded at the beginning and at the end of the immersion period in cell culture medium and ACSF. We found the phase angle of the impedance to be the most sensitive parameter for monitoring changes of the interface properties. A striking spectrum shift was observed during long-time immersion of the electrode in complex organic solutions (Fig. 8A). The alterations hint at an additional capacitive effect emerging within the system. This is significant—especially in the low frequency range. After 5 days in cell culture medium, the electrodes were extensively rinsed with distilled water. Nevertheless, this treatment was unable to restore the original impedance spectra. The electrodes were thus treated with pepsin to enzymatically clean the surface from protein films. Even though this procedure was almost successful in restoring the frequency behavior of the Pt/Ir electrodes (Fig. 8B), this was not the case with the stainless steel electrodes (Fig. 8C). Obviously, the remaining difference must be due to irreversible electrode change, especially corrosion.

3.6. Modeling the electrode impedance

The impedance of the electrode interface + medium system can qualitatively be modeled by combining resistive and capacitive elements. The equivalent circuit of Fig. 9 allows

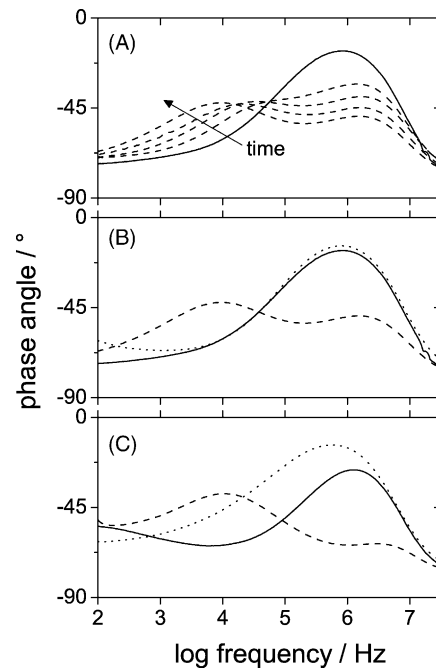


Fig. 8. Phase angle variation with immersion time in cell culture medium and after-treatment of electrodes: (A) time sequence for an S25-Pt/Ir electrode (starting at solid line: 0, 24, 32, 80, 120 h); the arrow indicates the progress in time; (B) S25-Pt/Ir electrode before (solid line) immersion for 5 days, after immersion (dashed line) and after pepsin treatment and thorough rinsing by distilled water (dotted line); (C) like (B) with an S75-SS electrode.

for a good description of the impedance behavior of immersed DBS electrodes.

In this illustration, resistors represent conductive paths, like the ionic bulk conductance, while capacitors are related to polarization or adsorption processes in interfacial electrochemical reactions. The medium impedance is presented by the parallel circuit of resistor R_E and capacitor C_E . This circuit accounts for the semicircles in Fig. 5 (please note that R_E has been determined from Fig. 5 and listed in Table 2). It describes a single dispersion process, namely the superseding of the Ohmic ionic current by the permittivity-based displacement current as frequency increases. Ideally, this process would have a single time constant and the semicircle centers would lie on the abscissa. In practice, the centers are usually located below the abscissa (see Fig. 5). The common inter-

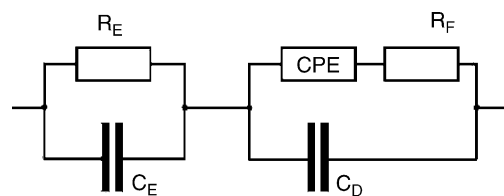


Fig. 9. Equivalent circuit used for modeling the electrode impedance. R_F , C_D , R_E , C_E , CPE stand for charge transfer resistance, double-layer capacitance, electrolyte resistance, electrolyte capacitance and the modified constant phase element (CPE). The CPE is described by Eq. (4). Electronically, it represents a serial cascade of parallel resistor–capacitor pairs with hierarchical parameters (Macdonald, 1987).

pretation for this behavior is the superposition of processes with distributed time constants leading to a superposition of distributed semicircles, which results in a flattening of the resultant arc (Schwan, 1968). Whereas the medium impedance dominates at high frequencies, the electrode–electrolyte interface dominates at low frequencies (see Fig. 5). In principle, the electrode–electrolyte interface can also be modeled by a resistor (R_F) in parallel to a capacitor (C_D) representing the polarization resistance due to the limited charge transfer through the interface and the electric double-layer capacitance. In order to account for the measured points distributed on a straight line, the circuit must model a semicircle of large radius. Nevertheless, the angle at which the experimental curve approaches the abscissa at increasing frequencies does not approach 90° as would be expected for a semicircle (Fig. 5; see also Fig. 6B). In practice, a straight line with a largely constant angle provides a better fit of the experimental points. Phenomenologically, this behavior can be interpreted as the superposition of numerous dispersion processes described by semicircles with increasing radii, i.e. increasing electrode impedance, for decreasing frequency. Mathematically, these properties can be described by non-linear circuit elements accounting for a non-ideal behavior of the capacitive and resistive elements. In Fig. 9 this behavior is described by the constant phase element (CPE). Its impedance is given by

$$Z_{CPE} = \frac{1}{G\omega^{1-m} + iQ\omega^m} \quad (4)$$

where ω , G , and Q are the circular frequency, the interfacial conductance, and the interfacial capacitance, respectively. m is the fractal exponent ($-1 \leq m \leq 1$). It describes the deviation of the interfacial impedance from the ideal behavior ($m = 1$). Intermediate values describe distributed properties of the capacitive and resistive elements.

Different model circuits have been tested to fit the measured impedance spectra (Figs. 5 and 6). The conformity of the fits has been judged with naked eye. The combination of the scheme in Fig. 9 with Eq. (4) was one of the models proposed by the LEVM 7.11 program (Solartron, J.R. Macdonald; www.solartronanalytical.com/downloads/software.html). It provided the best qualitative description combining the constant phase behavior with a semicircle at higher frequencies. It was therefore employed to fit the parameters of the circuit to the measured impedance spectra (Figs. 5 and 6) by a non-linear complex least square fit (results not shown).

According to Eq. (4), different fractal coefficients were obtained. We found only small differences for electrodes of the same geometry but made of different materials. Nevertheless, different geometries (electrode diameter, surface area, electrode distance, asymmetry) resulted in remarkable differences of all parameters of the CPE. C_D and R_F could be neglected when no bias voltage had been applied. To fit spectra measured with DC bias, non-zero parameters had to be assumed for C_D and R_F , allowing for a discontinuity in

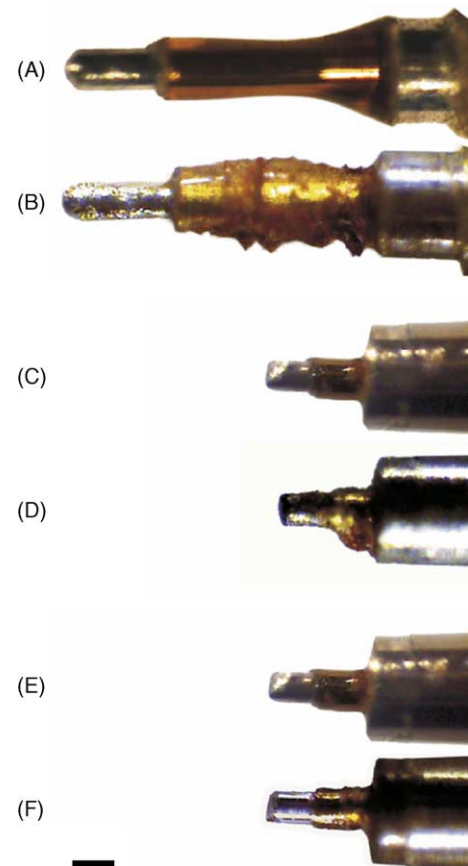


Fig. 10. Light microscopy images of three electrodes differing in geometry and/or material. Corrosion is more severe in stainless steel electrodes. (A and B) are stainless steel electrodes Sx(b) (SNEX-100) in new (A) and used (B) conditions, respectively. (C and D) are S75 made from stainless steel while electrodes in (E and F) have stainless steel outer poles and Pt/Ir inner poles, in new (C and E) and used (D and F) conditions, respectively. Interestingly, the extent of epoxy corrosion depends on the electrode material; compare (D and F). Corroded electrodes were in continuous use over more than 8 h. Scale bar: 100 μm .

the description of the electrode–electrolyte interface properties.

In long-term measurements, the fractal exponent decreased from about 0.66 to 0.47, reaching steady state after about 60 h (data not shown) suggesting that the electrode surfaces roughened (see also Figs. 10 and 11). At the steady state level, there was little difference in the parameters found for different electrode materials. This suggests that adsorption of organic molecules was at an equilibrium and further corrosion no longer altered the surface roughness.

In the constant-current mode, a larger electrode surface at the microscopic scale will lead to a lower current density through the electrode's surface. The larger effective surface area will also result in a higher specific capacitance and, consequently to a capacitive bridging of the electrode polarization already at lower frequencies. Hence, after long-term use of electrodes their increasing surface roughness might lead to a better capacitive bridging of the low frequency components necessary for DBS.

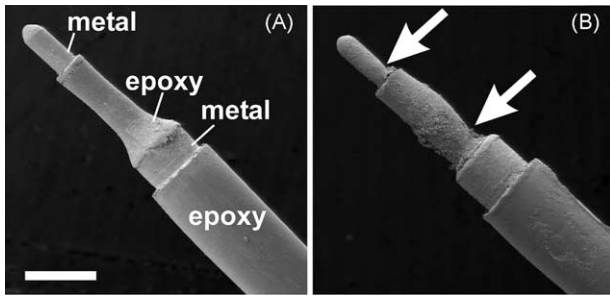


Fig. 11. Metal corrosion and epoxy erosion of stainless steel electrodes after continuous use for about 8 h. Note that both metal corrosion and epoxy erosion are especially abrasive at junctions of metal and insulation (arrows). Scanning electron micrographs of a new (A) and a used (B) stainless steel microelectrode (SNEX-100; Sx(b)). Scale bar: 300 μm .

3.7. Metal and epoxy corrosion

When applying electric fields in electrolyte solutions, such as interstitial fluid, different electrode processes may occur: gas evolution, redox-reactions of the organic solution compounds and dissolution of the electrode metal (Agnew and McCreery, 1990; Robblee and Rose, 1990).

As can be seen from Figs. 10 and 11, except for the metal part of the platinum electrode, both electrodes and the epoxy insulation show traces of corrosion after use.

4. Discussion

Parkinson's disease (PD) is characterized by a degeneration of the substantia nigra pars compacta, resulting in a striatal dopamine depletion, leading to motor deficits, such as bradykinesia, rigidity, postural instability and tremor. Since PD is associated with abnormal activity of the subthalamic nucleus (STN) (Robledo and Feger, 1991), one therapeutic option is to block STN neural activity (Bergman et al., 1990). STN lesions have been shown to alleviate motor deficits in monkey and rodent models of PD as well as in PD patients (Bergman et al., 1990; Aziz et al., 1991; Baunez et al., 1995; Henderson et al., 1999; Phillips and Brown, 1999). However, the lesions are irreversible and patients may suffer from side-effects. DBS was developed as a reversible alternative to surgical lesions following the observation that high-frequency stimulation (>100 Hz) of the thalamus "mimicked" the anti-tremor effects of a thalamic lesion (Benabid et al., 1987; Limousin et al., 1995).

Investigations in animal models are vital for improving DBS techniques and the theoretical understanding of them. The problems described here may in part play a role in the DBS treatment of patients. The stimulation voltage ranges between 0.8 and 8.0 V with a mean around 3.0 V for STN stimulation, and between 1.1 and 5.0 V, with a mean around 3.3 V for Globus pallidus internus (GPI) stimulation. The frequency ranges between 90 and 185 Hz for STN stimulation, and 80 and 185 Hz for GPI (The Deep-Brain Stimulation for

Parkinson's Disease Study Group, 2001). These parameters are in a range where we could detect strong non-linearities in current–voltage behavior as well as a significant influence by electrode processes on impedance.

4.1. DC-properties of electrodes

4.1.1. Electrode polarization and overpotential

Electrode polarization is the reason for the complex non-linear properties of electrodes. Metal electrodes are polarizable as a rule, i.e. for a certain DC current passing through the electrode a potential higher than the electrode's equilibrium potential has to be applied. This additional (or over) potential results from a number of different contributions (Vetter, 1961). The simplest of which, resistance polarization, describes the electrode's potential change due to the voltage drop over the medium according to Ohm's law. All other contributions are related to the complexity of the electrode process. Charge transfer polarizations are caused by the excess potential required to overcome activation energy barriers, such as the transition of charge carriers through the electric double-layer. Concentration polarizations are the result of concentration gradients of charge carriers or reactants near the electrode. An initial reason for concentration polarization may be the limited rate of reactant supply and/or product removal (diffusion polarization). Another possible cause may be that the electrode reaction itself or a subsequent reaction limit the rate of current transport (reaction polarization). Similarly, the removal or crystallization of metal ions from or to the metal lattice may limit the current flow (crystallization polarization). The total polarization, or overpotential, results from the sum of all contributions.

When electrodes are driven by a low frequency AC field the same polarization processes will occur in principle. Nevertheless, as frequency increases, the electrode processes are bridged. Capacitive bridging is due to the low thickness of the electric double-layer at the electrode surface where the polarization processes are located. DC-driven chemical reactions contribute to a lower electrode polarization at high frequencies since they need not be completed in order to allow an AC current to flow. This applies to reactions with reaction rates in the range of the field frequency. After bridging of all electrode processes, the current will only be limited by the medium conductance according to Ohm's law (see Fig. 4). The ionic medium current will be superseded by displacement currents when the frequency is increased even further (see later). As Fourier analysis showed, the stimulus applied in DBS contains a wide range of frequencies where polarization processes are relevant.

4.2. Macro- versus microelectrodes in complex solutions

In early experiments, we found that symmetrical electrodes of mm-dimensions could be characterized by standard

electronic means, which was not the case for the coaxial microelectrodes used in animal DBS. With DC the characteristic bending in the slope like in Fig. 4 around 2–3 V could not be detected clearly. Obviously, the small size of the electrodes with their sharp edges and a strong variation in surface curvatures (the inverse of the surface radii) influences their electric properties.

The strong variation in the curvatures results in a strong variation of the surface current densities, in turn leading to a variation of the surface properties. As a result, depending on site, the same electrode surface will conduct current with different characteristics. The effect can be explained by the following consideration: For a measuring chamber consisting of two coplanar electrodes of distance d and area A , filled by a medium of specific conductivity σ , the impedance Z is given by $Z = d/(\sigma A)$. When the electrode area is reduced, the same impedance can be obtained for an electrode distance itself reduced by the same factor. Nevertheless, when the current is kept constant, the current density through the electrodes will be increased, resulting in more intense electrode reactions. The higher intensity of the electrode reactions was one of the reasons for the non-reproducible and time-dependent current–voltage relation of microelectrodes in contrast to macroelectrodes. Electrode reactions caused the formation of bubbles and surface plaques.

We assume there are a number of reasons for asymmetry of the current function with respect to the polarity of the DC-bias. One will be the different metals for the central and the outer electrodes. Nevertheless, even for electrodes of the same material, a change in polarity will alter the current densities at the anode and cathode as the pole subject to the higher current density has changed. The situation is even more complicated when microelectrodes are immersed in interstitial fluid or media used in cell or tissue cultures, since organic and highly complex macromolecules of these solutions influence electrode behavior, for instance by the formation of protein films (Omanovic and Roscoe, 2000; Jackson et al., 2000).

4.3. AC-properties of electrodes

4.3.1. Electrode impedance

In a linear system, a sinusoidal voltage will induce a sinusoidal current of the same frequency. At any frequency the impedance can be calculated straight forward by Ohm's law from the ratio of voltage and induced current. In such a system, the time domain behavior can be constructed from the frequency domain behavior by inverse Fourier transformation. In other words, if the frequency responses (impedance) of the electrode and medium were known, the temporal current behavior in the medium could be predicted. The field in the medium will be proportional to the current.

Unfortunately, electrode systems are non-linear and a sinusoidal voltage generates a non-sinusoidal current. Furthermore, the non-linearity depends on the amplitude and current density of the driving voltage. Therefore, it is not pos-

sible to describe the current by means of a Fourier series, i.e. by the sum of current contributions of different amplitudes and frequencies induced by a voltage pulse in analogy to Eqs. (1)–(3). The waveform of the current signal and consequently its Fourier content will differ from the electrode voltage signal (Moussavi et al., 1994). Furthermore, electrochemical processes alter the electrode properties while measurement is taking place (cf. Fig. 7) as well as contribute to electrode aging over periods of hours and days (see later and Figs. 8, 10 and 11). An aggravating problem is the distribution of parameters such as current density along the electrode surface, leading to a site-dependent impedance.

The relative contribution of medium and electrode properties to impedance depends critically on frequency. The higher the frequency, the lower the contribution of electrode processes. For the Fourier frequency content of the DBS signal, gray matter has a conductivity of between 0.1 and 1 S/m (Gabriel et al., 1996; Schmid et al., 2003). As shown in Table 2, the frequencies at which electrode processes cease to influence the impedance range from hundreds of kHz up to the low MHz range for these conductivities. For frequencies below approximately 10 kHz, more than half of the signal amplitude is dissipated by electrode processes, which means that these parts of the Fourier spectrum do not stimulate the tissue but seriously threaten it by electrode processes and their by-products. Higher stimulation frequencies are therefore to be preferred. The effect might be an explanation for clinical observations that low-frequency DBS signals (10–50 Hz) did not have clinical effects and in a range of stimulus frequencies between 90 and 170 Hz, higher frequencies required less signal intensity to reach the same clinical effect and had fewer side-effects (Rizzone et al., 2001). However, we have to stress that for the non-linearity of the system, the calculations in Table 2 are merely qualitative estimations.

As Figs. 4 and 7 show, higher amplitudes result in a decrease in effective impedance, especially at low frequencies. An additional bias voltage also results in an increased current density and a reduced impedance. Probably, the bias can be assumed to contribute to the activation energies of the redox-reactions at the electrode. Summarizing, input signal amplitudes affect the waveform of the field which is induced in the tissue.

For non-coplanar electrodes, the local impedance depends on the local interfacial capacitance and local polarization resistance (overpotentials). Both parameters depend on the local current density. As a consequence, an electrode impedance distribution along the surface will be obtained depending on a combination of geometry and polarization effects. The impedance distribution at the electrode surface will lead to a smoothening of the current–voltage relation of the electrode and a broadening of the impedance spectrum. This effect is more pronounced for micro- than for macro-electrodes because of the stronger variation in current density along the surface encountered with them.

4.4. AC-properties of medium, tissue and electrodes

4.4.1. Medium and tissue impedance

Impedance spectroscopy provides information on the charge transition processes at the electrodes, as well as on the properties of media like electrolytes, cell suspensions or tissues. With increasing frequency, electrode processes are bridged and the medium properties start dominating the overall impedance (see Table 1). Aqueous electrolytes are characterized by a frequency-independent specific ion conductivity and the permittivity of water (about 80 times the permittivity of vacuum) up to GHz frequencies. The overall current through the medium is the sum of ionic currents and the permittivity based displacement currents that are increasing with frequency, superseding the frequency-independent ionic currents above the so called Maxwell-Wagner frequency (about 300 MHz for physiological ionic strength). At the Maxwell–Wagner frequency ionic and displacement currents are balanced. In the complex plane the frequency dependence is reflected by a semicircle as known for the parallel circuit of resistor and capacitor (Fig. 5). In an ideal case, its center would lay on the abscissa, reflecting a single dispersion process with a single time constant. The time constant corresponds to the frequency of the point above the semicircle center, representing the Maxwell–Wagner frequency. Semicircle centers below the abscissa like in Fig. 5 are caused by a superposition of processes representing a distribution of time constants.

When the medium contains organic molecules or even cells both, conductivity and permittivity will become frequency dependent. The medium properties will be characterized by a typical decrease in permittivity and a corresponding increase in conductivity with increasing frequency (see dispersion curve, (Foster and Schwan, 1997)). The amplitudes of the dispersions are proportional to the concentration of molecules or cells. Regardless of their high concentration in organic molecules, for simplicity dispersions of cytoplasmic or interstitial media are usually neglected.

4.4.2. Current–voltage characteristics and medium field

In homogeneous media the local current density is directly related to the local field. For electrodes, only at very low amplitudes (or high frequencies) can a linear current response be expected, even when harmonic sinusoidal voltage signals are applied. Larger amplitudes will result in a non-linear current–voltage response and the generation of higher harmonics (Schwan and Onaral, 1985; Moussavi et al., 1994). The degree of non-linearity depends on frequency. A qualitative description of the frequency-dependence of the current–voltage relation of macroelectrodes could be obtained by neglecting the distortions in the signal shape (Fig. 4). Above a certain frequency the bridging of electrode processes leads to a linear behavior. The lowest frequency of linear behavior (around 1 kHz in Fig. 4) depends on electrode geometry (area and distance for two coplanar electrodes),

current density, medium composition, electrode material and surface properties.

Two factors determine the local field distribution in the vicinity of the electrode surface; the overall electrode shape (which would fully determine the local current density and thus spatial field distribution in the ideal case of no electrode processes, e.g. at high frequencies) and the current density at all given sites of the electrode surface (which determines the local polarization impedance, modulating the local current densities). The latter implies that electrode material and medium or tissue composition influence the field distribution in tissue.

Fig. 7B (inset) is characterized by the decomposition/redox potential of solution components, like organic compounds in the case of cell culture medium. As in Fig. 4, the observed behavior suggests that low frequency input signals will be deformed. The impedance–voltage and current–voltage relations are asymmetric for the two voltage branches. This means that for a given voltage, different currents will be measured when the inner or outer poles of the electrode are used as the cathode (or anode). This effect can be explained by the different surface areas of the anode and cathode of the concentric bipolar electrodes. Consequently, current densities as well as electrode polarization effects will differ and the question of which electrode is driven as cathode (or anode) will be significant.

Another interesting consideration is that a rectangular constant-current pulse through the electrode will not necessarily induce a rectangular field pulses at all electrode sites. Because of the impedance distribution along the electrode surface, different electrode sites may exhibit different current wave shapes, resulting in different time functions of the field in the vicinity of the electrode surface. Nevertheless, the different local surface current contributions must add up to the rectangular current input.

4.4.3. Passive cell membrane properties represent a high frequency cut-off for DBS

The DBS signal is influencing neuronal activity by the induction of a transmembrane potential ($\Delta\psi$) on these cells. For the comparatively low potentials (a few mV) required for the induction of an action potential, generally, a linear relation of the induced potential to the field strength can be assumed. $\Delta\psi$ can be calculated analytically for cells of ellipsoidal or cylindrical shape with low membrane conductivities immersed in media of homogeneous electric properties (Gimsa and Wachner, 2001a; Gimsa and Wachner, 2001b). $\Delta\psi$ is given by $\delta r E$, where δ , r , and E stand for the shape factor, the length of the cellular semiaxis oriented in field direction and the external field strength, respectively. For a spherical cell, δ is 1.5. The limiting values for δ are 1 and 2 that are assumed for cylindrical cells along and perpendicular to their symmetry axis, respectively. To avoid irreversible membrane and cell damage, it is important to keep $\Delta\psi$ below 1 V. For increasing frequency $\Delta\psi$ is declining with a characteristic dependence

on frequency f :

$$\Delta\psi = \frac{\delta r E}{\sqrt{1 + f^2/f_{\text{char}}^2}} \quad (5)$$

At frequencies far below f_{char} Eq. (5) simplifies to $\Delta\psi = \delta r E$. At field strengths of 667 and 333 V/m, a $\Delta\psi$ of 10 mV is induced for spherical cell bodies of 5 and 10 μm radius, respectively. For a cylindrical axon of 0.5 μm radius, a field strength of 10,000 V/m is required when the symmetry axis of the axon is perpendicularly oriented to the field. The above calculations do not necessarily implicate a prominent somatic effect of DBS since (i) due to their different active electric properties, the threshold for stimulating axons is much lower than for stimulating cell bodies and (ii) the frequency window for axonal stimulation is much broader (see later). Therefore our considerations are not contradictory to the experimental and modeling evidence that the action potential occurs in the axon during extracellular stimulation (Nowak and Bullier, 1998; McIntyre and Grill, 1999).

With increasing field frequency $\Delta\psi$ drops, reaching -3dB , i.e. $\delta r E/\sqrt{2}$ at the characteristic frequency f_{char} . Please note that the time constant of membrane charging by an externally applied field, $1/(2\pi f_{\text{char}})$, considered here, is much shorter than the membrane time constant observed in a whole cell configuration. Neglecting the membrane conductivity f_{char} is given by (Gimsa and Wachner, 2001a):

$$f_{\text{char}} = \frac{1}{2\pi r C_m} \frac{\sigma_e \sigma_i}{\sigma_e + (\delta - 1)\sigma_i} \quad (6)$$

with C_m , σ_e and σ_i standing for the specific membrane capacitance as well as the external and internal conductivities, respectively. Assuming C_m to be 0.9 $\mu\text{F}/\text{cm}^2$, and varying the cell radius from 5 to 10 μm as well as σ_e and σ_i in the ranges of 1–1.5 and 0.5–1 S/m (Gabriel et al., 1996; Gentet et al., 2000; Schmid et al., 2003), respectively, yielded limiting values for the characteristic frequencies of the spherical cell soma between 707 kHz ($r = 10 \mu\text{m}$, $\sigma_e = 1 \text{ S/m}$, $\sigma_i = 0.5 \text{ S/m}$) and 2.65 MHz ($r = 5 \mu\text{m}$, $\sigma_e = 1.5 \text{ S/m}$, $\sigma_i = 1 \text{ S/m}$), respectively. For axons of a radius of 0.5 μm , the same conductivity variations yielded limiting values between 11.8 MHz ($\sigma_e = 1 \text{ S/m}$, $\sigma_i = 0.5 \text{ S/m}$) and 21.2 MHz ($\sigma_e = 1.5 \text{ S/m}$, $\sigma_i = 1 \text{ S/m}$), respectively.

These values are merely rough estimates for an assumed cell-free, homogeneous external surrounding. The embedding of the cell in tissue will lower the effective external conductivity to be assumed in Eq. (6). At the same time, the tissue will introduce frequency-dependent properties for the external medium (see earlier). For $\sigma_e = 0.05 \text{ S/m}$, a lower limit for the characteristic frequency of 147 kHz is obtained for a spherical cell soma of 10 μm radius and $\sigma_i = 0.5 \text{ S/m}$. Fig. 2 shows that rectangular pulses of 130 Hz contain only minute amplitudes above 130 kHz. Nevertheless, cutting the frequencies above 130 kHz for the monophasic rectangular pulse (Fig. 2A) results in the pulse shape of Fig. 3D, demonstrating that already slightly higher stimulation frequencies

or shorter pulse widths may lead to a capacitive membrane bridging of the high frequency components of the pulse and a corresponding energy loss in neuronal stimulation. As shown before (Figs. 5 and 6), electrode properties do impose a low frequency limit, reducing the amplitudes of low frequency components in the tissue. The two contributions will result in a frequency window for DBS.

4.4.4. Long-term alterations of electrodes and tissue damage

Electrode properties are subject to aging driven by metal corrosion, erosion of the insulating material and deposition of organic and inorganic compounds at the electrode. A comparison of electrodes immersed in electrolyte or cell culture medium with and without a stimulation signal revealed a drift of the electrode properties, different in either case. Therefore, a drift of the electrode properties during electrostimulation cannot fully be avoided by a post-operational resting time of the implanted electrode. Metal corrosion, occurring even with no stimulation signal, is increased during electrostimulation. Since the surface current density reflects the rates of electrochemical reactions at the electrode–electrolyte interface it is related to corrosion and erosion kinetics. Corrosion may result in the ablation of electrode material and, in the extreme, a decrease in the mechanical stability of the electrode (Kocijan et al., 2003). The changes we found within hours imply that stimulation parameters should be readjusted, even at the short application times in animal models.

For the corrosion effect, it is probably of importance as to whether the two poles of the coaxial electrodes are electrically cut short by the stimulator during the signal off-time. Especially, since they are made of two different materials which form an electrochemical element. These effects will be not so important in patients, since the poles of electrodes for use in humans are made of the same material. Nevertheless, it cannot be ruled out that the different coverage and/or corrosion of poles with different history will mimic different electrode materials.

The adsorption of organic species at the metal surface is a third effect causing property changes of the metal–electrolyte interfaces. This bio-layer formation reduces the transport of ions, oxygen and dissolution products to and away from the surface decreasing the slope in the corresponding Tafel-plot, i.e. decreasing the exchange current density (compare cell culture medium and ACSF, inset of Fig. 7B) (Contu et al., 2002). Protein adsorption may also enhance corrosion resistance (Robblee and Rose, 1990). This is in line with our finding that long-term immersion caused changes in electrode properties that were irreversible for ACSF but could largely be reversed for cell culture medium (data not shown). It is also in line with the more negative corrosion potential in serum-containing than in serum-free media (Contu et al., 2002). Accordingly, the rate of cathodic oxygen reduction in serum is lower than in inorganic solution. The rate of protein adsorption was found to increase with voltage (Brusatori et al., 2003). All these findings suggest that during DBS in ani-

mal models and patients, protein adsorption processes occur even faster than in our experiments, since we applied lower voltages for shorter periods of time or immersed the electrodes even without stimulation.

On the other hand, electrode adsorption of organic compounds will be related to changes in the tissue. Corrosion will result in the deposition of electrode metal in the brain. Metal ions are known to be a potential source of protein-denaturation and the formation of new antigenic determinants leading to immune reactions (Zitter and Plenk, 1987). Especially iron is known for its cytotoxicity (Smythies, 1999). The degradation of organic compounds, the evolution of gas, such as hydrogen, oxygen and chlorine are non-physiological processes changing the properties of the extracellular fluid. Such changes are known to cause neuronal damage (McCreery and Agnew, 1990). Even cell necrosis caused by irreversible dielectric membrane breakdown must be expected at field hot spots in the vicinity of the electrode surface.

Corrosion resistance of the electrode metal is of greatest importance for its long-term stability and biocompatibility. Naturally, less noble metals will be subject to stronger corrosion. Pt and Pt/Ir alloys are the most common electrode materials for their electrical, mechanical and chemical properties as well as their biocompatibility (Robblee and Rose, 1990). Accordingly, we found the strongest effects for stainless steel electrodes with the clear formation of corrosion pits. The electrode surface did not corrode uniformly. Instead, we found a spatial distribution of the corrosion and erosion intensities reflecting the site dependence of the current density (Figs. 10 and 11, data of numerical calculations not shown). Erosion of the plastics insulation is a severe problem since the putative biological effects of these erosion products have not been described so far.

4.5. Comparison with the human situation—relevance in clinical use

This study focuses on electrodes used in rodent models. However, the question arises as to the extent our findings apply to the clinical practice of DBS in patients. Direct transferability is unlikely, as electrodes for use in patients and animal models differ in principal electrode design, i.e. a number of equal ring electrodes in humans and two coaxial electrodes in animals, as well as size and materials, both of poles and insulation. In addition, stimulation protocols differ, i.e. constant-voltage stimulation is used in humans while constant-current stimulation is commonly applied in rodents. Current densities critically depend on electrode shape and size. Therefore, simply down-sizing the electrodes while maintaining the same stimulation parameters would result in serious tissue damage. Nevertheless, some basic features apply to both situations.

The signals used contain frequencies that are unable to stimulate neurons while being lost in electrochemical processes, such as gas formation due to electrode polarization processes. Although corrosion has not been observed with the electrodes used in patients, such electrochemical processes

are unavoidable. This teaches us two lessons: first, electrodes for animal models should be designed to match the materials used in humans; second, stimulation parameters for humans as well as animal models should be reconsidered so as to reduce the energy of the low and high frequency components of the stimulation signal that is dissipated by electrode processes and capacitively bridged by the membranes. Since corrosion is an indicator of electrode processes, it emphatically suggests a problem that cannot be unique to animal models. Our study revealed the basis for a number of different processes that will also occur in the clinical situation, although without the drastic effects described here.

5. Conclusion and outlook

The focus of this study has been on the electrical and electrochemical properties of microelectrodes used in DBS animal experiments. A comparison of electrodes immersed in electrolyte or cell culture medium with and without a stimulation signal revealed a drift of the electrode properties which was different in all cases and which was also dependent on the electrode material. With platinum electrodes, the property drift could be largely reversed by pepsin treatment, though this was not the case with stainless steel electrodes. The property drift may make it necessary to adjust the stimulation parameters in medical applications. Moreover, our data suggests that stimulation parameters should also be readjusted in animal models—despite the usually shorter application—since reversible and irreversible changes in electrode properties take place within hours.

The tissue field distribution depends on electrode geometry. Along the electrode surface, the field strength is correlated to the current density distribution which corresponds to the intensity of electrochemical processes and in turn the corrosion rate. Numerical calculations of the influence of electrode geometries on the field distribution in the tissue and on the current density at the electrode surface are currently underway (manuscript in preparation). Nevertheless, the calculations must assume a linear electrode behavior. Site-dependencies of impedance and the non-linearity in the current–voltage relation cannot easily be included in numerical calculations. Despite this uncertainty, even a rough analysis of the local current density distribution at the electrode surface and in the surrounding tissue will help in deciding whether the neurons are uniformly influenced and whether the electrodes will corrode uniformly.

The sites of maximum plastics erosion can also be correlated in relation to current density. Both processes (metal corrosion and plastics erosion) contribute to the deposition in the brain tissue of putative neurotoxic compounds, such as dissolved electrode metal, reactive compounds stemming from the erosion of the insulating material, evolved gas, as well as degraded organic molecules. The use of stainless steel electrodes does not match the situation with humans. To avoid animals suffering unnecessarily we recommend the

use of platinum/iridium electrodes. Future electrode development needs to improve the electrode geometry to avoid current density “hot spots” and involve the search for more inert insulating materials.

A 130 Hz monophasic DBS standard pulse of 60 μ s has a Fourier content of more than three frequency decades. Its frequency band is located in a window imposed by the electrode properties at the low frequency end and capacitive membrane bridging at the high frequency end. Of course, the complex morphology and the active electric properties of the neurons also impose an upper limit. Nevertheless, the low frequency end is more critical since low frequency pulse components contribute to electrode processes. Electrode impedance measurements on S75-Pt/Ir microelectrodes in NaCl solution, ACSF and cell culture medium suggest that even though electrode processes are reduced at higher frequencies they only disappear completely above 1 MHz and cannot be avoided in the present system. In conclusion, stimulation frequencies and pulse widths should be selected so that the frequency components of the Fourier series are as high as possible.

Acknowledgements

This study has been supported by grants 01 ZZ 0108 of the Bundesministerium für Bildung und Forschung to U.G. and StSch 20020418A of the Bundesamt für Strahlenschutz to J.G. We are grateful for help of the core facility “electron microscopy” of the medical faculty of the University of Rostock.

References

- Agnew WF, McCreery DB. Neural prostheses: fundamental studies. Englewood Cliffs, NJ: Prentice-Hall; 1990.
- Atkins PW. Physical chemistry. 4th ed. Oxford: Oxford University Press; 1991.
- Aziz TZ, Peggs D, Sambrook MA, Crossman AR. Lesion of the subthalamic nucleus for the alleviation of 1-methyl-4-phenyl-1,2,3,6-tetrahydropyridine (MPTP)-induced parkinsonism in the primate. *Mov Disord* 1991;6:288–92.
- Baunez C, Nieoullon A, Amalric M. In a rat model of parkinsonism, lesions of the subthalamic nucleus reverse increases of reaction time but induce a dramatic premature responding deficit. *J Neurosci* 1995;15:6531–41.
- Benabid AL, Pollak P, Louveau A, Henry S, de Rougemont J. Combined (thalamotomy and stimulation) stereotactic surgery of the VIM thalamic nucleus for bilateral Parkinson disease. *Appl Neurophysiol* 1987;50:344–6.
- Bergman H, Wichmann T, DeLong MR. Reversal of experimental parkinsonism by lesions of the subthalamic nucleus. *Science* 1990;249:1436–8.
- Bressand K, Dematteis M, Ming GD, Vercueil L, Louis BA, Benazzouz A. Superior colliculus firing changes after lesion or electrical stimulation of the subthalamic nucleus in the rat. *Brain Res* 2002;943:93–100.
- Bruet N, Windels F, Bertrand A, Feuerstein C, Poupard A, Savasta M. High frequency stimulation of the subthalamic nucleus increases the extracellular contents of striatal dopamine in normal and partially dopaminergic denervated rats. *J Neuropathol Exp Neurol* 2001;60:15–24.
- Brusatori MA, Tie Y, Van Tassel PR. Protein adsorption kinetics under an applied electric field: An optical waveguide lightmode spectroscopy study. *Langmuir* 2003;19:5089–97.
- Chang JY, Shi LH, Luo F, Woodward DJ. High frequency stimulation of the subthalamic nucleus improves treadmill locomotion in unilateral 6-hydroxydopamine lesioned rats. *Brain Res* 2003;983:174–84.
- Contu F, Elsener B, Bohni H. Characterization of implant materials in fetal bovine serum and sodium sulfate by electrochemical impedance spectroscopy. Part I. Mechanically polished samples. *J Biomed Mater Res* 2002;62:412–21.
- Darbaky Y, Forni C, Amalric M, Baunez C. High frequency stimulation of the subthalamic nucleus has beneficial antiparkinsonian effects on motor functions in rats, but less efficiency in a choice reaction time task. *Eur J Neurosci* 2003;18:951–6.
- Fleischmann M, Pons S, Hawkins M, Hoffman RJ. Measurement of gamma-rays from cold fusion. *Nature* 1989;339:667.
- Foster KR, Schwan HP. Dielectric properties of tissues—a review. Boca Raton, FL: CRC Press; 1997.
- Fung SH, Burstein D, Born RT. In vivo microelectrode track reconstruction using magnetic resonance imaging. *J Neurosci Methods* 1998;80:215–24.
- Gabriel C, Gabriel S, Corthout E. The dielectric properties of biological tissues. Part I. Literature survey. *Phys Med Biol* 1996;41:2231–49.
- Gentet LJ, Stuart GJ, Clements JD. Direct measurement of specific membrane capacitance in neurons. *Biophys J* 2000;79:314–20.
- Gimsa J, Wachner D. Analytical description of the transmembrane voltage induced on arbitrarily oriented ellipsoidal and cylindrical cells. *Biophys J* 2001a;81:1888–96.
- Gimsa J, Wachner D. On the analytical description of transmembrane voltage induced on spheroidal cells with zero membrane conductance. *Eur Biophys J* 2001b;30:463–6.
- Haberler C, Alesch F, Mazal PR, Pilz P, Jellinger K, Pinter MM, Hainfellner JA, Budka H. No tissue damage by chronic deep brain stimulation in Parkinson's disease. *Ann Neurol* 2000;48:372–6.
- Henderson JM, Annett LE, Ryan LJ, Chiang W, Hidaka S, Torres EM, Dunnett SB. Subthalamic nucleus lesions induce deficits as well as benefits in the hemiparkinsonian rat. *Eur J Neurosci* 1999;11:2749–57.
- Henderson JM, Pell M, O'Sullivan DJ, McCusker EA, Fung VS, Hedges P, Halliday GM. Postmortem analysis of bilateral subthalamic electrode implants in Parkinson's disease. *Mov Disord* 2002;17:133–7.
- Jackson DR, Omanovic S, Roscoe SG. Electrochemical studies of the adsorption behavior of serum proteins on titanium. *Langmuir* 2000;16:5449–57.
- Kocijan A, Milosev I, Pihlar B. The influence of complexing agent and proteins on the corrosion of stainless steels and their metal components. *J Mater Sci Mater Med* 2003;14:69–77.
- Limousin P, Pollak P, Benazzouz A, Hoffmann D, Le Bas JF, Broussolle E, Perret JE, Benabid AL. Effect of parkinsonian signs and symptoms of bilateral subthalamic nucleus stimulation. *Lancet* 1995;345:91–5.
- Macdonald JR. Impedance spectroscopy—emphasizing solid materials and systems. New York, Chichester, Brisbane, Toronto, Singapore: Wiley; 1987.
- McCreery DB, Agnew WF. Mechanisms of stimulation-induced neural damage and their relation to guidelines for safe stimulation. Englewood Cliffs, NJ: Prentice-Hall; 1990.
- McIntyre CC, Grill WM. Excitation of central nervous system neurons by nonuniform electric fields. *Biophys J* 1999;76:878–88.
- Meissner W, Paul G, Reum T, Reese R, Sohr R, Morgenstern R, Kupsch A. The influence of pallidal deep brain stimulation on striatal dopaminergic metabolism in the rat. *Neurosci Lett* 2000;296:149–52.
- Meissner W, Reum T, Paul G, Harnack D, Sohr R, Morgenstern R, Kupsch A. Striatal dopaminergic metabolism is increased by deep brain stimulation of the subthalamic nucleus in 6-hydroxydopamine lesioned rats. *Neurosci Lett* 2001;303:165–8.

- Moser A, Gieselberg A, Ro B, Keller C, Qadri F. Deep brain stimulation: response to neuronal high frequency stimulation is mediated through GABA(A) receptor activation in rats. *Neurosci Lett* 2003;341:57–60.
- Moussavi M, Schwan HP, Sun HH. Harmonic distortion caused by electrode polarisation. *Med Biol Eng Comput* 1994;32:121–5.
- Nowak LG, Bullier J. Axons, but not cell bodies, are activated by electrical stimulation in cortical gray matter. Part II. Evidence from selective inactivation of cell bodies and axon initial segments. *Exp Brain Res* 1998;118:489–500.
- Omanovic S, Roscoe SG. Interfacial behavior of beta-lactoglobulin at a stainless steel surface: an electrochemical impedance spectroscopy study. *J Colloid Interf Sci* 2000;227:452–600.
- Paul G, Reum T, Meissner W, Marburger A, Sohr R, Morgenstern R, Kupsch A. High frequency stimulation of the subthalamic nucleus influences striatal dopaminergic metabolism in the naive rat. *Neuroreport* 2000;11:441–4.
- Phillips JM, Brown VJ. Reaction time performance following unilateral striatal dopamine depletion and lesions of the subthalamic nucleus in the rat. *Eur J Neurosci* 1999;11:1003–10.
- Rizzone M, Lanotte M, Bergamasco B, Tavella A, Torre E, Faccani G, Melcarne A, Lopiano L. Deep brain stimulation of the subthalamic nucleus in Parkinson's disease: effects of variation in stimulation parameters. *J Neurol Neurosurg Psychiatry* 2001;71:215–9.
- Robblee LS, Rose TL. Electrochemical guidelines for selection of protocols and electrode materials for neural stimulation. Englewood Cliffs, NJ: Prentice-Hall; 1990.
- Robledo P, Feger J. Acute monoaminergic depletion in the rat potentiates the excitatory effect of the subthalamic nucleus in the substantia nigra pars reticulata but not in the pallidal complex. *J Neural Transm Gen Sect* 1991;86:115–26.
- Schmid G, Neubauer G, Mazal PR. Dielectric properties of human brain tissue measured less than 10 h postmortem at frequencies from 800 to 2450 MHz. *Bioelectromagnetics* 2003;24:423–30.
- Schwan HP. Electrode polarization impedance and measurements in biological materials. *Ann NY Acad Sci* 1968;148:191–209.
- Schwan HP, Onaral B. Linear and nonlinear properties of platinum-electrode polarization. Part 3. Equivalence of frequency-domain and time-domain behavior. *Med Biol Eng Comput* 1985;23:28–32.
- Smythies J. The neurotoxicity of glutamate, dopamine, iron and reactive oxygen species: functional interrelationships in health and disease: a review-discussion. *Neurotox Res* 1999;1:27–39.
- The Deep-Brain Stimulation for Parkinson's Disease Study Group. Deep-brain stimulation of the subthalamic nucleus or the pars interna of the globus pallidus in Parkinson's disease. *N Engl J Med* 2001;345:956–63.
- Vetter KJ. *Elektrochemische Kinetik*. Berlin, Göttingen, Heidelberg: Springer Verlag; 1961.
- Windels F, Bruet N, Poupard A, Feuerstein C, Bertrand A, Savasta M. Influence of the frequency parameter on extracellular glutamate and gamma-aminobutyric acid in substantia nigra and globus pallidus during electrical stimulation of subthalamic nucleus in rats. *J Neurosci Res* 2003;72:259–67.
- Windels F, Bruet N, Poupard A, Urbain N, Chouvet G, Feuerstein C, Savasta M. Effects of high frequency stimulation of subthalamic nucleus on extracellular glutamate and GABA in substantia nigra and globus pallidus in the normal rat. *Eur J Neurosci* 2000;12:4141–6.
- Zitter H, Plenk H. The electrochemical behavior of metallic implant materials as an indicator of their biocompatibility. *J Biomed Mater Res* 1987;21:881–96.